https://doi.org/10.1007/s41230-026-5201-7

Regulating creep behavior via dynamic in-situ precipitation of Ti_3AlC phase in Ti45Al8Nb-0.6C alloy

Zhe Deng[1, 2, 3], *Pei Liu[1, 3, 4], Wei Wang[1, 3, 4], Ai-qin Wang[1, 3, 4], Jing-pei Xie[1, 3, 4], and **Zhi-yong Zhang[2]

1. College of Materials Science and Engineering, Henan University of Science and Technology, Luoyang 471023, Henan, China

2. State Key Laboratory of Advanced Casting Technologies, Shenyang 110022, China

3. State Key Laboratory of Light Superalloys, Henan University of Science and Technology, Luoyang 471023, Henan, China

4. Provincial and Ministerial Co-construction of Collaborative Innovation Center for Non-ferrous Metal New Materials and Advanced Processing Technology, Luoyang 471023, Henan, China

Abstract: TiAl alloys are attractive for high-temperature structural applications, yet their creep resistance and microstructural stability at high temperatures remain critical challenges. In this study, Ti45Al8Nb-0.6C alloy was prepared by vacuum induction melting to investigate its creep behavior and underlying deformation mechanisms at 800 °C under 200 MPa. The alloy exhibits a relatively homogeneous microstructure composed of (γ+α_2) lamellar colonies, B2 phase, and blocky γ phase, with a creep life of 137 h and a typical ductile-brittle mixed fracture mode. Post-creep microstructural characterization reveals pronounced B2 phase formation, deformation twinning, lamellar coarsening, and abundant stacking faults at lamellar interfaces. Extensive dynamic recrystallization occurs during creep, leading to the formation of fine recrystallized grains. The Ti_3AlC phase plays a dual strengthening role by effectively impeding dislocation motion and developing characteristic defect structures, including high-density dislocations and ladder-like stacking faults during deformation. These synergistic microstructural evolutions contribute to the enhanced creep resistance of the alloy.

Keywords: high Nb-TiAl; microstructure; creep properties; deformation mechanism

CLC numbers: TG146.23 **Document code:** A **Article ID:** 1672-6421(2026)03-377-08

1 Introduction

TiAl-based intermetallic alloys have emerged as promising lightweight structural materials for aerospace applications due to their exceptional combination of high specific strength, superior oxidation resistance, and excellent high-temperature mechanical properties[1-4]. A significant milestone in commercialization is achieved with the successful implementation of Ti-48Al-2Cr-2Nb alloy in GEnx™ engine low-pressure turbine (LPT) blades, demonstrating its engineering viability for critical rotating components[5]. The growing demand for next-generation aeroengines with higher thrust-to-weight ratios, extended service life, and improved fuel efficiency has driven intensive research on developing advanced TiAl alloys with enhanced high-temperature capabilities[6]. However, broader applications of these alloys remain constrained by their limited high-temperature strength and creep resistance under extreme service conditions[7]. Recent advances in microstructure engineering have revealed that near-lamellar microstructures exhibit particularly outstanding high-temperature strength and creep performance[8-10]. These specially designed microstructures maintain adequate ductility while effectively impeding dislocation motion and grain boundary sliding at elevated temperatures, offering new opportunities for developing next-generation high-performance TiAl alloys.

Alloying has been widely recognized as an effective strategy for enhancing the properties of TiAl-based

***Pei Liu**

Male, born in 1991, Ph. D., Professor. His research interests primarily focus on the design and optimization of advanced high-temperature structural materials including Ti and TiAl alloys for aerospace.

E-mail: liupei@haust.edu.cn

****Zhi-yong Zhang**

E-mail: ustbamm2011@126.com

Received: 2025-08-20; Revised: 2025-10-08; Accepted: 2025-11-05

alloys[11-14]. Zhou et al.[15] developed Ti-46Al-2.6C-*x*Nb [*x*=(0–4)at.%] alloys using ultrasonic-assisted vacuum arc remelting (VAR). Their results demonstrated that increasing the Nb content from 0 to 4at.% significantly improved the ultimate compressive strength from 2,074 MPa to 2,474 MPa and concurrently increased the fracture strain from 23% to 28%. In a complementary study, Wang et al.[16] successfully fabricated Ti-45Al-8Nb alloy using arc-directed energy deposition (DED), revealing that Nb addition not only effectively reduced internal defects but also substantially enhanced mechanical properties through combined solid solution strengthening, grain refinement, and dislocation strengthening effects when compared with binary Ti-45Al alloy. These findings collectively highlight the crucial role of Nb alloying in optimizing both the processing characteristics and mechanical performance of TiAl alloys.

Although Nb is an effective β-stabilizing element in TiAl alloys, excessive addition can promote the formation of brittle B2 phase, leading to reduced ductility[17-19]. Recent studies[20, 21] have shown that this detrimental effect can be counteracted by incorporating α-stabilizing elements such as carbon. Beyond compensating for the negative impact of β-stabilizers, carbon addition independently enhances TiAl alloy performance through multiple mechanisms[22]. Carbon exhibits limited solid solubility in TiAl alloys, and when its content exceeds ~0.5at.%, it preferentially forms Ti_2AlC (H-phase) and Ti_3AlC (P-phase)[23, 24]. Li et al.[25] systematically investigated this phenomenon in Ti-43Al-6Nb-1Mo-1Cr-*x*C [*x*=(0–1.0)at.%] alloys prepared by induction skull melting (ISM). Advanced TEM and HRTEM characterization revealed that P-Ti_3AlC phases maintain a coherent interface with the γ-matrix, facilitating stress transfer while minimizing interface cracking. These precipitates were found to enhance plastic deformation capability by promoting dislocation glide and mechanical twinning, ultimately leading to improved strength and ductility in high-Nb TiAl alloys.

The individual roles of Nb and C in TiAl alloys have been extensively studied. However, the in-situ formation of the Ti_3AlC phase via the vacuum induction melting (VIM), particularly its dynamic precipitation behavior during high-temperature creep and the associated interaction mechanisms with microstructural defects such as dislocations and stacking faults, remains insufficiently understood. This study systematically investigates the optimization mechanism of graphite additives on the mechanical properties of high Nb-TiAl alloy. A Ti45Al8Nb-0.6C alloy was successfully developed and prepared via VIM, its high-temperature creep performance was systematically evaluated. The incorporation of graphite powder facilitates the in-situ formation of carbide reinforcements. An in-depth characterization of the microstructural evolution of TiAl alloys before and after deformation was conducted. By integrating high-temperature creep performance testing and fracture morphology analysis, this study elucidates the interfacial coordinated deformation mechanism between the carbide reinforcement phases and the matrix, and identifies the primary strengthening and toughening mechanisms.

2 Experimental procedure

High-purity starting materials were employed, including titanium sponge (99.7% purity), aluminum rods (99.99%), an aluminum-niobium master alloy (55wt.% Nb content), and graphite powder (99.98%). The vacuum induction melting (VIM) process was carried out under a high-purity argon protective atmosphere, which was introduced when the base vacuum level dropped below 5×10^{-4} Pa. To achieve optimal microstructural uniformity, the ingot underwent three successive remelting cycles. The resulting ingot had a diameter of 150 mm and a height of 80 mm. Subsequently, test samples were taken from predetermined locations of the homogenized ingot for characterization.

Microstructural characterization was performed using field emission scanning electron microscopy (FE-SEM, Hitachi SU8010) to analyze the deformed structures. For nanoscale investigation, transmission electron microscopy (TEM, FEI Tecnai G2 F30) was employed with bright-field imaging, energy-dispersive X-ray spectroscopy (EDS), and selected-area electron diffraction (SAED) techniques. Metallographic specimens were mechanically ground to #2000 grit, polished, and chemically etched using Kroll's reagent (5vol.% HF+10vol.% HNO_3+85vol.% H_2O). TEM samples were prepared by wire-electrode cutting, mechanically thinned to below 50 μm, and subsequently electropolished with a twin-jet system using an electrolyte of CH_3OH, $CH_3(CH_2)_3OH$, and $HClO_4$ in a volume ratio of 6:3:1. Creep tests were conducted on a universal testing machine under constant conditions of 800 °C and 200 MPa until specimen failure. Three thermocouples were strategically positioned along the upper, middle, and lower sections of the specimen for continuous temperature monitoring, to maintain the experimental temperature within acceptable error limits throughout testing.

3 Results and discussion

Figure 1 presents the microstructure of the Ti45Al8Nb-0.6C alloy. The alloy exhibits a typical lamellar architecture composed predominantly of alternating γ-TiAl and α_2-Ti_3Al lamellae, as shown in Fig. 1(a). The corresponding SAED pattern in Fig. 1(c) confirms the crystallographic orientation relationship between the γ-TiAl and α_2-Ti_3Al phases as $[1\bar{1}0]\gamma//[11\bar{2}0]\alpha_2$. Further insight into the interfacial atomic arrangement is provided by the IFFT image of the yellow-framed region in Fig. 1(b), presented in Fig. 1(d). In addition, the microstructure also contains the B2 phase and a small amount of γ phase distributed along the grain boundaries, as illustrated in Fig. 1(e), while the corresponding SAED pattern in Fig. 1(f) further confirms the presence of the B2 phase. This special phase distribution characteristic is mainly closely related to the alloy composition and solidification process. Nb, as a strong β-phase stabilizing

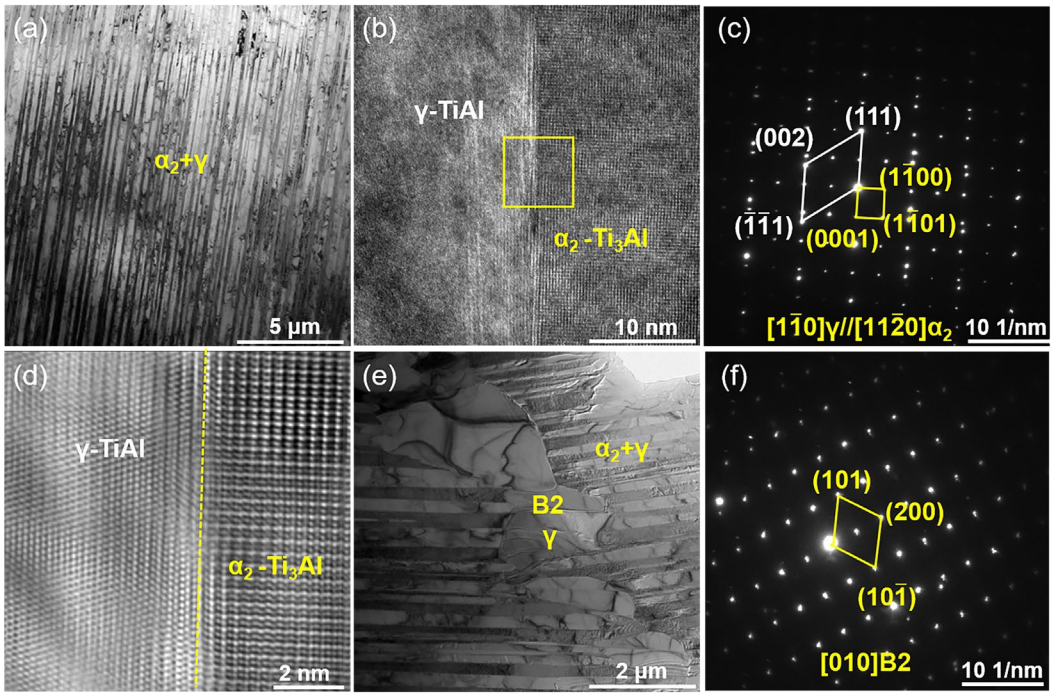

Fig. 1: Microstructure characterization of Ti45Al8Nb-0.6C alloy: (a) TEM image of α_2/γ phase; (b) HRTEM image of α_2/γ phase; (c) SAED image of α_2/γ phase; (d) IFFT image of α_2/γ phase; (e) TEM image of Ti45Al8Nb-0.6C alloy; (f) SAED image of B2 phase

element, can inhibit the formation of α-phase during the solidification process of the alloy and induce the ordering transformation of the high-temperature β-phase during cooling, which ultimately results in the formation of the B2-phase at room temperature. In addition, the addition of C further changes the solidification path of the alloy and promotes the phase equilibrium in the region of high Al content, resulting in the formation of a (B2+γ) mixed-phase structure at the grain boundaries.

Under creep conditions of 800 °C and 200 MPa, the strain-time curve of the Ti45Al8Nb-0.6C alloy is presented in Fig. 2(a). Correspondingly, the alloy exhibits a creep lifetime of 137 h and a steady-state creep rate of 6.4×10^{-8} s^{-1}. A comprehensive comparison of creep performance between the developed Ti45Al8Nb-0.6C alloy and various other TiAl alloys/composites[26-34] is illustrated in Fig. 2(b). As shown in Fig. 2(b), the creep resistance of the Ti45Al8Nb-0.6C alloy is comparable to, or even superior to, that of the reported high-Nb TiAl alloys with similar compositions. This enhanced performance can be primarily attributed to the role of carbon.

The deformation microstructures after creep exposure at 800 °C were further examined by TEM (Fig. 3). Along the ($\gamma+\alpha_2$) lamellae, irregularly shaped B2 phases are distributed in Fig. 3(a), while dislocations are uniformly distributed within the γ-phase grains. Deformation twinning within the γ phase is clearly observed in Fig. 3(b), and the corresponding SAED pattern in Fig. 3(c) confirms the twinning relationship. Additionally, Fig. 3(d) demonstrates the occurrence of bifurcation dissolution in the α_2 phase. Figures 3(e) and (f) highlight a high density of dislocations in the lamellae, along with pronounced dislocation entanglement. This observation suggests that dislocation slip serves as the primary deformation mechanism within the lamellae. Previous studies

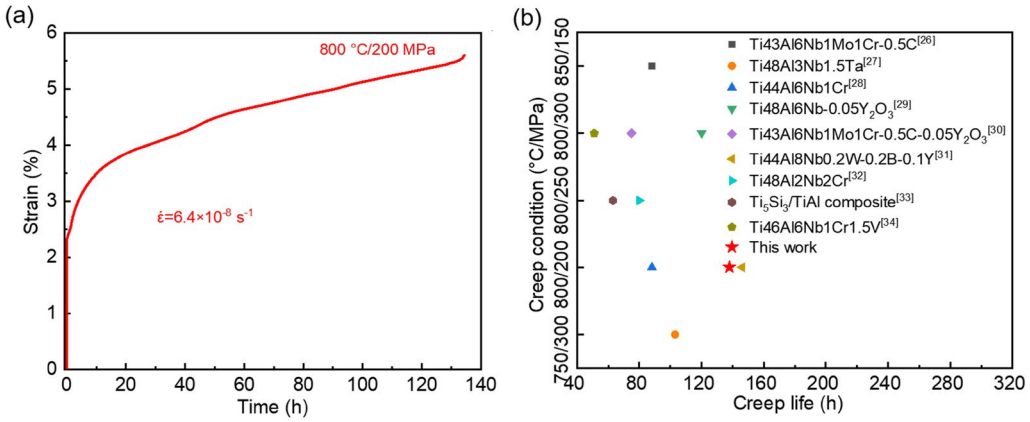

Fig. 2: High-temperature creep properties of Ti45Al8Nb-0.6C alloy at 800 °C under 200 MPa (a) and comparison of creep properties of Ti45Al8Nb-0.6C alloy with other reported TiAl alloys or composites (b)

have confirmed that high-temperature deformation activates a significant number of dislocations[35]. The interfacial dislocations observed here originate from mismatch stresses at γ/γ or γ/α_2 interfaces, where coherent stresses promote their formation to accommodate lattice misfit. Such interfacial dislocations are known to enhance the mechanical properties of composites.

Figure 4 provides further insight into the microstructural evolution induced by creep deformation. As illustrated in Fig. 4(a), a significant number of fine recrystallized grains are observed along the grain boundaries of the original lamellar colonies, providing clear evidence for the activation of dynamic recrystallization (DRX) during high-temperature deformation. A detailed examination of the yellow-marked region in Fig. 4(b) reveals a uniform distribution of dislocations within these newly formed grains, suggesting that plastic deformation persists even after recrystallization. Interestingly, some recrystallized grains are found to nucleate and grow directly from the lamellae, as shown in Fig. 4(c). In addition to recrystallization, Fig. 4(d) highlights another

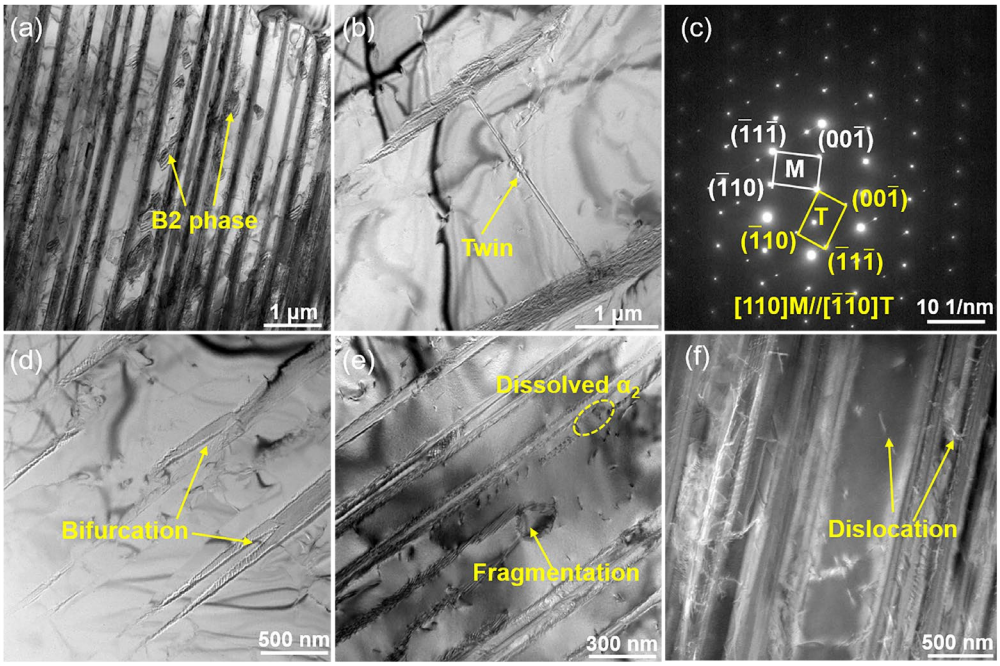

Fig. 3: Deformation characteristics of Ti45Al8Nb-0.6C alloy at 800 °C: (a) TEM image of B2 phase; (b) TEM image of twin in γ-TiAl; (c) SAED pattern of twin in (b); (d–e) TEM images of the degraded lamellar microstructure; (f) TEM image of dislocations in γ-TiAl

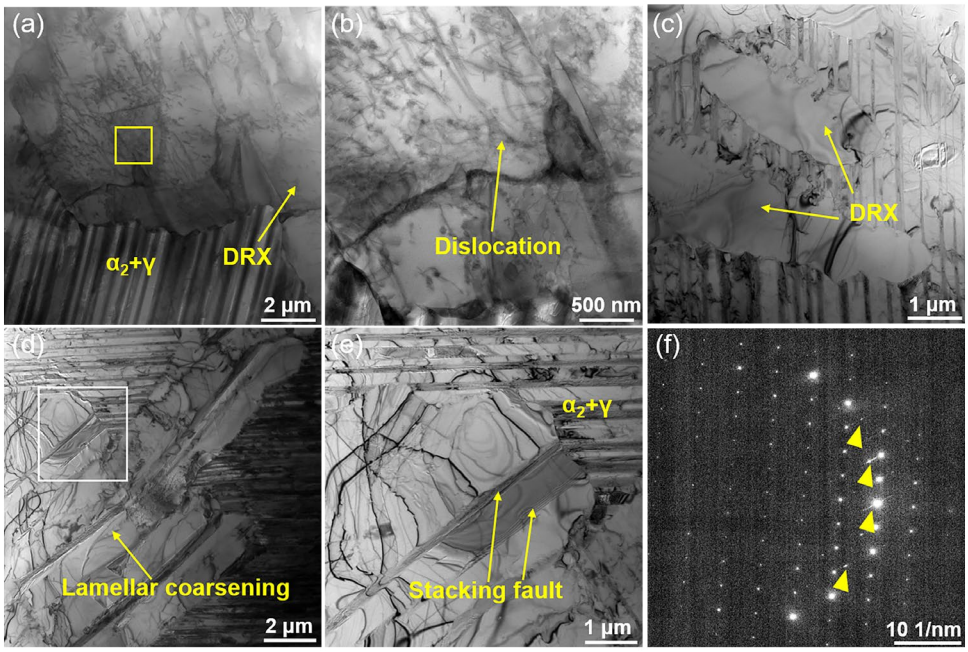

Fig. 4: Deformation characteristics of Ti45Al8Nb-0.6C alloy at 800 °C: (a–c) TEM images of dynamic recrystallization in TiAl alloy; (d) TEM image reveals the coarsened lamellar structure; (e) enlarged view of the white-box region in (d); (f) SAED pattern of γ-TiAl in (e)

critical microstructural change, the coarsening of lamellar colonies, which is a typical phenomenon during prolonged exposure to elevated temperatures. Further high-magnification analysis in Fig. 4(e) uncovers the presence of extensive stacking faults at the interfaces of the coarsened lamellar structures, indicating that interfacial defects play a crucial role in the deformation and coarsening mechanisms. The presence of these stacking faults is further confirmed by the streaking features in the corresponding SAED pattern [Fig. 4(f)].

After creep deformation at 800 °C/200 MPa, the morphology of Ti_3AlC in the Ti45Al8Nb-0.6C alloy is presented in Fig. 5. As shown in Fig. 5(a), the recrystallized grains exhibit a high density of dislocations along with numerous precipitates. Figure 5(b) provides a magnified view of the yellow rectangular region marked in Fig. 5(a), revealing extensive precipitated phases distributed along these dislocations. Further characterization of the precipitates is presented in Figs. 5(c) and (d), which display the SAED pattern and HRTEM image, respectively. The combined analysis of these figures confirms that the precipitated phase is Ti_3AlC. The corresponding IFFT image in Fig. 5(e) indicates that dislocations are also present within the Ti_3AlC precipitates themselves, while the geometric phase analysis (GPA) result in Fig. 5(f) reveals pronounced stress fluctuations at the Ti_3AlC/γ-phase interface. These precipitates play a critical role in obstructing dislocation motion, thereby significantly enhancing the creep resistance of the alloy. Furthermore, previous studies have demonstrated that elastic interactions between carbon atoms and dislocations lead to the formation of Cottrell atmospheres, which effectively pin dislocation motion[36]. To overcome this pinning effect, elevated local stresses are required. Consequently, solute carbon atoms enhance the alloy's creep resistance by increasing the critical resolved shear stress for dislocation glide.

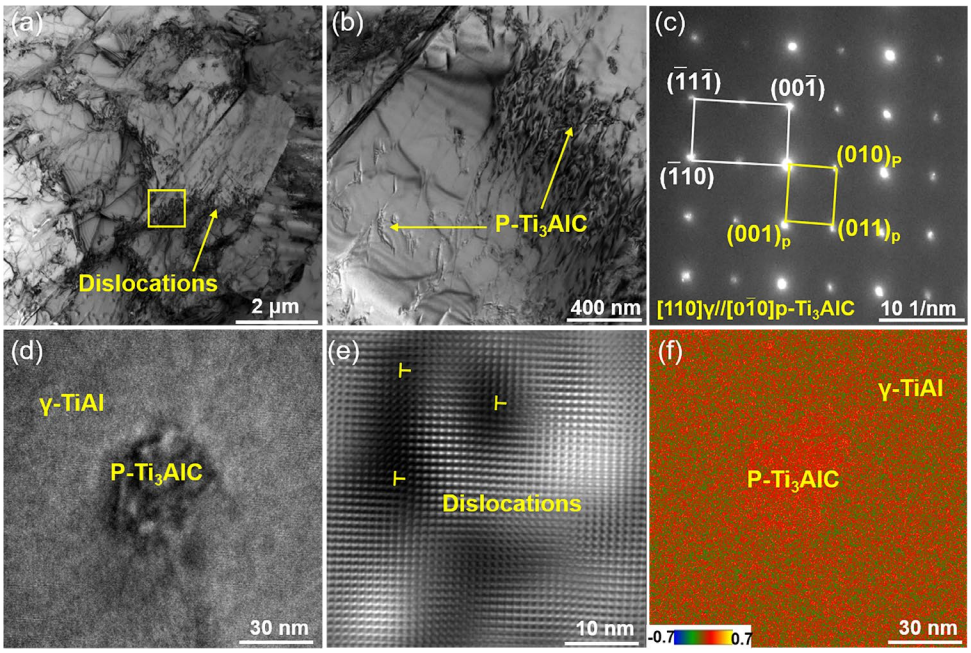

Fig. 5: Deformation characteristics of Ti_3AlC in Ti45Al8Nb-0.6C alloy at 800 °C: (a–b) BF image of Ti_3AlC phase; (c) SAED image of Ti_3AlC phase; (d) HRTEM image of Ti_3AlC/TiAl phase; (e) IFFT image of Ti_3AlC phase; (f) GPA image of Ti_3AlC/TiAl phase

Figure 6 further elucidates the interaction between deformation twins and Ti_3AlC precipitates under creep conditions. An HRTEM image in Fig. 6(a) captures the evolution path of twins formed under an applied load of 800 °C/200 MPa. Figure 6(b) shows the EDS elemental mapping of the region in Fig. 6(a), demonstrating that the carbides are segregated within the central region at the junction of the two twins. The diffraction spots in Fig. 6(c4) can be indexed to the Ti_3AlC phase, while Figs. 6(c1)–(c4) present the corresponding FFT patterns of the twin crystals and the Ti_3AlC region. Figures 6(d) and (e) present the IFFT images of the yellow- and green-marked regions in Fig. 6(a), respectively. A high density of crystallographic defects is observed at the interfaces between intersecting twins, as shown in Fig. 6(a). Notably, Twin 2 maintains a straight morphology without significant distortion even after intersecting with Twin 1. The IFFT analysis in Fig. 6(d) reveals distinct atomic disorder zones at both the Twin 1/Twin 2 interface and the interfaces between the twins and the Ti_3AlC phase, accompanied by a high density of dislocations.

Moreover, Fig. 6(e) shows that Ti_3AlC itself contains a large number of dislocations and stacking faults, some of which display a characteristic step-like configuration. These observations are consistent with previous findings by Wang et al.[37], who reported that Ti_3AlC can be sheared by dislocations, leading to the formation of stacking faults and intersecting stacking fault configurations. At 800 °C, enhanced local atomic rearrangement mitigates the nearest-neighbor violation around complex stacking faults, thereby promoting the formation of stacking faults in Ti_3AlC. Specifically, the glide of partial dislocations facilitates the propagation of stacking faults along the {111} planes, which subsequently interact to form

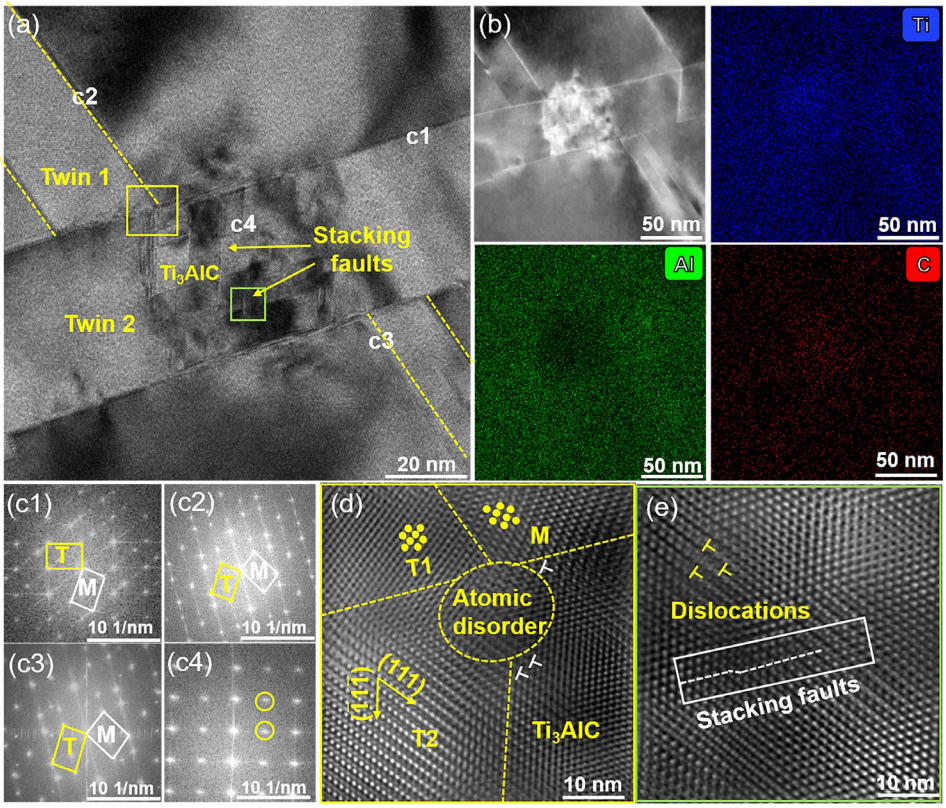

Fig. 6: Deformation characteristics of Ti_3AlC in the Ti45Al8Nb-0.6C alloy at 800 °C: (a) typical HRTEM image of the deformed Ti_3AlC at 800 °C; (b) corresponding element distribution in (a); (c1–c4) FFT image of HRTEM in (a); (d) IFFT image of the yellow-box region in (a); (e) IFFT image of the green-box region in (a)

intersecting stacking fault configurations. The resulting step-like arrangement may further strengthen the precipitates by acting as effective barriers to dislocation motion, rendering Ti_3AlC a potent obstacle to dislocation glide at elevated temperatures.

A comprehensive fractographic analysis was conducted to clarify the fracture behavior of the Ti45Al8Nb-0.6C alloy, as shown in Fig. 7. The fracture surfaces in Figs. 7(a)–(c) exhibit typical mixed ductile–brittle characteristics, including cleavage steps, river patterns, and shallow dimples. Particularly, Fig. 7(c) reveals that these dimples exhibit limited depth, which can be attributed to the carbide-hindered formation of B2/γ interfaces during creep deformation. Since dimples preferentially nucleate at B2/γ interfaces, the presence of carbides restricts interface formation, thereby resulting in shallow dimple morphologies. The crack propagation path, revealed by BSE images in Figs. 7(d)–(f), is accompanied by several microstructural evolution features such as microcracking, lamellar bending, and crack branching. In the early stage of propagation, cracks preferentially advance

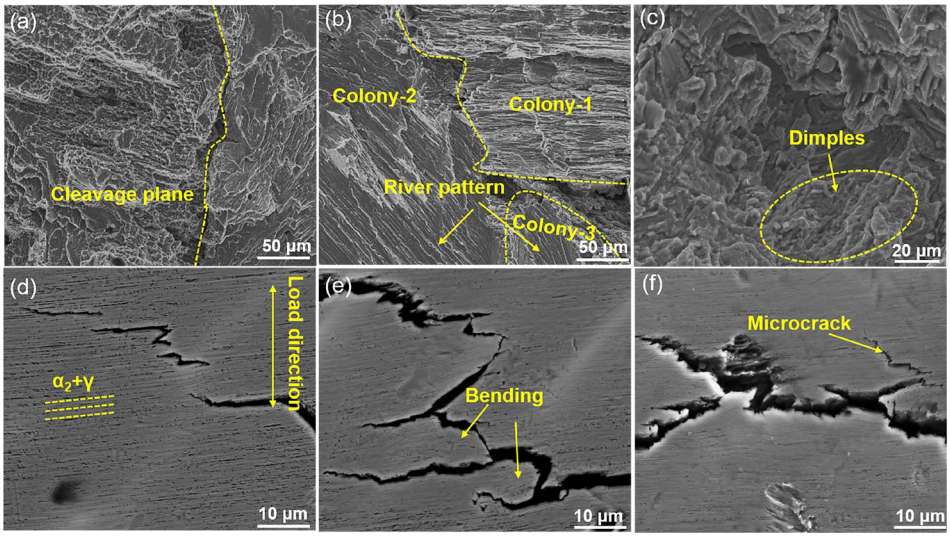

Fig. 7: Fracture morphology of Ti45Al8Nb-0.6C alloy (a–c) and BSE images of crack propagation in Ti45Al8Nb-0.6C alloy (d–f)

along α_2/γ interfaces, whereas pronounced crack deflection and branching occur at later stages. These sophisticated crack propagation mechanisms effectively alleviate stress concentration at the crack tip through stress field redistribution, thereby remarkably retarding the final fracture process.

Figure 8 schematically illustrates the creep-induced microstructural evolution in Ti45Al8Nb-0.6C alloy. From the figure, it can be seen that for the Ti45Al8Nb-0.6C alloy, the microstructure consists of ($\alpha_2+\gamma$) lamellar colonies with B2 phase and blocky γ phase, where the B2 phase alternates with the blocky γ phase. During creep exposure, carbon diffusion facilitates the formation of the Ti_3AlC phase, which acts as an effective barrier to dislocation motion and substantially enhances creep resistance. Simultaneously, unique defect configurations develop within the precipitates, including high-density dislocations and terraced stacking faults, contributing to the thermal stability and strengthening capability of Ti_3AlC at elevated temperatures. Post-deformation characterization reveals substantial dynamic recrystallization and secondary B2 phase precipitation. In addition, crack propagation exhibits preferential orientation perpendicular to the loading axis, with effective stress dissipation achieved through crack deflection and microcrack branching phenomena.

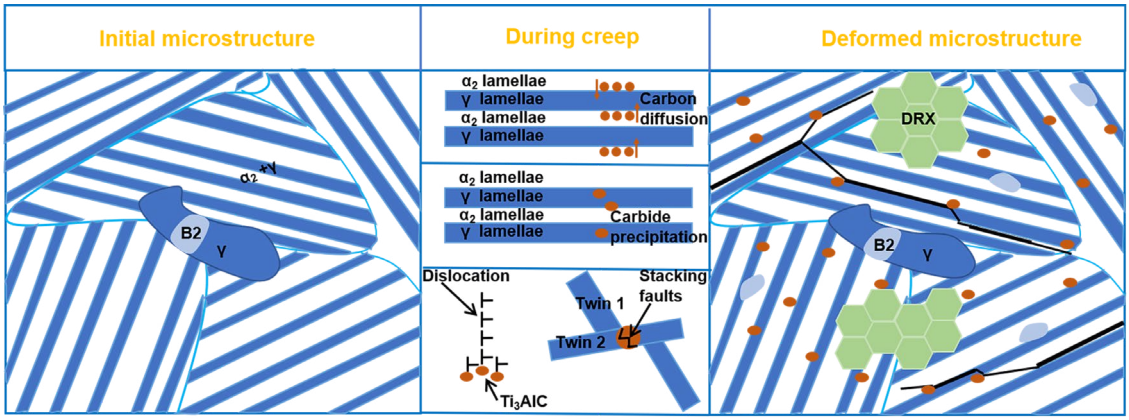

Fig. 8: Schematic diagram illustrating the effect of microstructure evolution on creep resistance of Ti45Al8Nb-0.6C alloy

4 Conclusions

In this study, Ti45Al8Nb-0.6C composite was fabricated by the VIM method, and its microstructural development was thoroughly investigated. Mechanical property assessments were performed, and the associated deformation mechanisms were analyzed, culminating in the subsequent conclusions:

(1) The Ti45Al8Nb-0.6C alloy fabricated via VIM exhibits a well-defined microstructure comprising (γ-TiAl+α_2-Ti_3Al) lamellae, B2 phase, and blocky γ phase with alternating distribution. This unique microstructure contributes to exceptional creep resistance, demonstrating a remarkable creep life of 137 h under demanding conditions of 800 °C/200 MPa.

(2) The Ti45Al8Nb-0.6C alloy shows mixed ductile-brittle fracture features, with cracks growing perpendicular to the loading direction. After deformation, the microstructure changes significantly, forming B2 phase, twins, and stacking faults, while also undergoing recrystallization during creep.

(3) The enhanced creep resistance originates from the effects of Ti_3AlC phase, which serve dual functions: effectively impeding dislocation motion while developing unique defect configurations including high-density dislocations and ladder-like stacking faults. These microstructural modifications collectively contribute to the superior high-temperature performance of the alloy system.

Acknowledgments

This work was financially supported by the open research fund of State Key Laboratory of Advanced Casting Technologies (Grant No. CAT2023-007), the National Natural Science Foundation of China (Grant No. 52571170), the Key Research and Development Program in Henan Province (Grant No. 242102230059), and the Natural Science Foundation of Henan Province (Grant No. 252300421326).

Conflict of interest

The authors declare that they have no known competing financial interests or personal relationships that could have appeared to influence the work reported in this paper.

References

[1] Wang S P, Zhu D M, Lu Z T, et al. Designing high ductility TiAl alloys based on dislocation nucleation mechanism. Acta Materialia, 2025, 292: 121027.

[2] Liang Z Q, Xiao S L, Li Q C, et al. Creep behavior and related phase precipitation of a creep-resistant Y_2O_3-bearing high Nb containing TiAl alloy. Materials Characterization, 2023, 198: 112767.

[3] Wang Q B, Zhang S Z, Zhang C J, et al. The influence of the dynamic softening mechanism of α phase and γ phase on remnant lamellae during hot deformation. Journal of Alloys and Compounds, 2021, 872: 159514.

[4] Ding H, Cui X P, Gao N N, et al. Fabrication of (TiB/Ti)-TiAl composites with a controlled laminated architecture and enhanced mechanical properties. Journal of Materials Science and Technology, 2021, 62: 221–233.

[5] Deng Z, Chen Z X, Wang Y P, et al. In-situ synthesized multi-component particle reinforced TiAl composite with excellent mechanical properties. Materials Today Communications, 2024, 38: 108060.
[6] Chen Y, Liu G H, Wang Y, et al. Solidification microstructure of Ti-43Al alloy by twin-roll strip casting. China Foundry, 2023, 20(2): 99–107.
[7] Yang W G, Li M A, Zhou T, et al. Deformation behavior and dynamic recrystallization mechanism of a novel high Nb containing TiAl alloy in (α+γ) dual-phase field. Journal of Alloys and Compounds, 2023, 945: 169250.
[8] Li K X, Fang H Z, Liang J S, et al. Forming Ru containing eutectoid structure serves as the dislocation storage unit at the lamellar colony boundary of TiAl alloy. Acta Materialia, 2024, 285: 120587.
[9] Chen Z X, Deng Z, Wang Y P, et al. Solidification behavior of TiB_2-Ti_2AlN reinforced TiAl composites with variation Al content. Intermetallics, 2025, 178: 108640.
[10] Wang D P, Chen G, Wang A D, et al. Corrosion behavior of single- and poly-crystalline dual-phase TiAl-Ti_3Al alloy in NaCl solution. International Journal of Minerals Metallurgy and Materials, 2023, 30: 689–696.
[11] Sun Y Y, Chen F, Qian S W, et al. Microstructure evolution mechanism of Fe microalloying high Nb-TiAl alloy fabricated by HIP. Journal of Materials Research and Technology, 2025, 36: 1273–1282.
[12] Liu X, Song L, Stark A, et al. Deformation and phase transformation behaviors of a high Nb-containing TiAl alloy compressed at intermediate temperatures. Journal of Materials Science and Technology, 2022, 102: 89–96.
[13] Guo X, Zhao Y J, Song L, et al. Phase transformation mechanisms of hP18 and ω_o phases in Zr and Hf containing high Nb-TiAl alloys. Journal of Alloys and Compounds, 2025, 1018: 179214.
[14] Lin X J, Huang H J, Yuan X G, et al. High temperature oxidation behavior of a cast Ti-47.5Al-2.5V-1.0Cr-0.2Zr alloy. China Foundry, 2022, 19(5) : 443–454.
[15] Zhou L Y, Fang H Z, Chen R R, et al. Effects of niobium and ultrasonic action coupling on microstructure evolution and mechanical properties of Ti46Al2.6C alloy. Journal of Alloys and Compounds, 2022, 904: 164048.
[16] Wang Z, Chen W, Chen Z W, et al. Enhanced mechanical properties of TiAl alloy through Nb alloying by triple-wire arc directed energy deposition. Journal of Materials Processing Technology, 2025, 339: 118800.
[17] Wimler D, Lindemann J, Kremmer T, et al. Microstructure and mechanical properties of novel TiAl alloys tailored via phase and precipitate morphology. Intermetallics, 2021, 138: 107316.
[18] Qiang F M, Kou H C, Tang B, et al. Effect of cooling rate on microstructure evolution of Ti-45Al-8.5Nb-0.2W-0.2B-0.02Y alloy during multi-step heat treatment. Materials Characterization, 2018, 145: 210–217.
[19] Yang G, Kou H C, Yang J R, et al. Microstructure control of Ti-45Al-8.5Nb-(W, B, Y) alloy during the solidification process. Acta Materialia, 2016, 112: 121–131.
[20] Wang Z B, Liu P, Wang A Q, et al. Fabrication, microstructure and mechanical properties of TiAl matrix composite reinforced by submicro/nano-Ti_2AlC. Materials Characterization, 2023, 203: 113141.
[21] Liu P, Wang Z B, Ye F, et al. Hierarchically heterogeneous strategy for Ti_2AlC/TiAl composite with superior mechanical properties. Composites, Part B: Engineering, 2024, 273: 111259.
[22] Lapin J, Pelachová T, and Bajana O. High temperature deformation behaviour and microstructure of cast in-situ TiAl matrix composite reinforced with carbide particles. Journal of Alloys and Compounds, 2019, 797: 754–765.
[23] Menand A, Huguet A, and Nérac-Partaix A. Interstitial solubility in γ and α_2 phases of TiAl-based alloys. Acta Materialia, 1996, 44: 4729–4737.
[24] Scheu C, Stergar E, Schober M, et al. High carbon solubility in a γ-TiAl based Ti-45Al-5Nb-0.5C alloy and its effect on hardening. Acta Materialia, 2009, 57: 1504–1511.
[25] Li M A, Xiao S L, Xu L J, et al. Microscale investigation of perovskite-Ti_3AlC strengthening and plastic deformation in high niobium containing TiAl alloys. Journal of Alloys and Compounds, 2021, 857: 157563.
[26] Tian Y, Li Q C, Liang Z Q, et al. Enhanced creep properties and creep-induced microstructure evolution behavior of carbon-doped TiAl alloys. Intermetallics, 2025, 181: 108749.
[27] Zuo Z B, Hu R, Li S Q, et al. A novel Ta-contained TiAl alloy with excellent high temperature performance designed for powder hot isostatic pressing. Journal of Alloys and Compounds, 2024, 1008: 176706.
[28] Wang Q, Chen R R, Yang Y H, et al. Improvement of the creep lifetimes and microstructural stability of β-solidifying γ-TiAl by cold crucible directional solidification. Intermetallics, 2018, 100: 104–111.
[29] Guo Y F, Xiao S L, Tian J, et al. Creep deformation and rupture behavior of a high Nb containing TiAl alloy reinforced with Y_2O_3 particles. Materials Characterization, 2021, 179: 111355.
[30] Liang Z Q, Xiao S L, Yu H B, et al. Enhanced high temperature tensile and creep properties of a β-solidified γ-TiAl alloy with the hybrid addition of C and Y_2O_3. Intermetallics, 2022, 150: 107698.
[31] Tian S G, Wang Q, Yu H C, et al. Microstructure and creep behaviors of a high Nb-TiAl intermetallic compound based alloy. Materials Science and Engineering: A, 2014, 614: 338-346.
[32] Yue H Y, Liang Z Q, Zhang F, et al. Effect of heat treatment on the microstructure and creep properties of Ti-48Al-2Cr-2Nb alloy produced by selective electron beam melting. Materials Science and Engineering: A, 2022, 859: 144224.
[33] Zhang Y Y, Cui X P, Zhai X X, et al. Significant enhancement in high temperature performance of TiAl matrix composites by a novel configuration design. Materials Science and Engineering: A, 2024, 889: 145872.
[34] Liang Z Q, Xiao S, Li X Y, et al. Significant improvement in creep resistance of Ti-46Al-6Nb-1Cr-1.5V alloy via introducing high-density nanotwins. Materials Science and Engineering: A, 2023, 862: 144485.
[35] Liu J H, Wang Z M, Li P, et al. Fabrication of high strength TiAl alloy with nano-lamellar and ultra-fine-grained microstructure by selective electron beam melting. Journal of Materials Research and Technology, 2025, 35: 7156–7166.
[36] Sun M H, Nie X, Chen Z W, et al. Improved low-stress thermoplastic forming of TiAl alloys via dislocation behavior under mechanical vibration. Journal of Alloys and Compounds, 2025, 1022: 180030.
[37] Wang L, Liang X P, Liu B, et al. Stacking fault formation in perovskite Ti_3AlC carbides in a TiAl based alloy during creep at 800 °C. Scripta Materialia, 2023, 222: 115034.